Some Integral Geometry Tools to Estimate the Complexity of 3D Scenes

Frédéric Cazals, Mateu Sbert

INSTITUT NATIONAL DE RECHERCHE EN INFORMATIQUE ET EN AUTOMATIQUE

Some Integral Geometry Tools to Estimate the Complexity of $3D$ Scenes

F.Cazals and M.Sbert

[1]Algorithms project, INRIA Rocquencourt, F-78153 Le Chesnay
[2]Institut d'Informàtica i Aplicacions, Universitat de Girona, Av. Lluis Santaló s/n, 17071, Girona, Spain.
emails: Frederic.Cazals@inria.fr, mateu@ima.udg.es

N ° 3204

Juillet 1997

THÈME 2

ISSN 0249-6399

INRIA
ROCQUENCOURT

Some Integral Geometry Tools to Estimate the Complexity of $3D$ Scenes

F.Cazals and M.Sbert

[1]Algorithms project, INRIA Rocquencourt, F-78153 Le Chesnay
[2]Institut d'Informàtica i Aplicacions, Universitat de Girona, Av. Lluis Santaló s/n, 17071, Girona, Spain.
emails: Frederic.Cazals@inria.fr, mateu@ima.udg.es

Thème 2 — Génie logiciel
et calcul symbolique
Projet Algorithmes

Rapport de recherche n°3204 — Juillet 1997 — 19 pages

Abstract: Many problems in computer graphics deal with complex $3D$ scenes where visibility, proximity, collision detection queries have to be answered. Due to the complexity of these queries and the one of the models they are applied to, data structures most often based on hierarchical decompositions have been proposed to solve them. As a result of these involved algorithms/data structures, most of the analysis have been carried out in the worst case and fail to report good average case performances in a vast majority of cases.

The goal of this work is therefore to investigate geometric probability tools to characterize average case properties of standard scenes such as architectural scenes, natural models, etc under some standard visibility and proximity requests. In the first part we recall some fundamentals of integral geometry and discuss the classical assumption of measures invariant under the group of motions in the context of non uniform models. In the second one we present simple generalizations of results describing the interactions between random lines and planes, and random bodies. And in the third one we report experimental results obtained for five fairly complex real-world models. These results exhibit a very good match between the theory and the practice, thus giving credit to the scene model used all along.

Key-words: Average case analysis, Stochastic geometry, Computer graphics

(Résumé : tsvp)

Quelques outils de géométrie intégrale pour caractériser la complexité de scènes $3D$

Résumé : De nombreux problèmes en infographie consistent à répondre à des requêtes de proximité ou de visibilité sur des scènes $3D$ complexes. Étant donnée la complexité de ces requêtes et celle des modèles auxquels elles sont appliquées, des structures de données basées le plus souvent sur des décompositions hiérarchiques ont été proposées. L'analyse de celles-ci s'effectuant dans le cas le pire, elle inapte à capturer de bonnes performances en moyenne.

Ce travail présente donc des outils de géométrie stochastique destinés à caractériser des propriétés en moyenne de requêtes de proximité, visibilité, etc., appliquées à des scènes classiques telles que les scènes architecturales ou les modèles naturels. Dans la première partie nous rappelons quelques résultats élémentaires de géométrie intégrale et en particulier montrons que l'hypothèse habituelle de mesures invariantes par le groupe des déplacements n'est pas incompatible avec des distributions d'objets non uniformes. Dans la seconde, nous présentons des statistiques décrivant l'interaction de droites et plans aléatoires avec des distributions arbitraires d'objets. Et dans la troisième nous validons ces résultats théoriques par des tests sur cinq scènes complexes.

Mots-clé : Analyse en moyenne, Géométrie stochastique, Infographie

1 Introduction

1.1 Non uniform distributions and global properties

To figure out the kind of properties we are interested in we start by reviewing two problems arising in the lightnings methods of radiosity and ray-tracing.

As is well known, the core computation of radiosity consists in computing the so-called form factors between the patches discretizing the scene. This process is inherently quadratic in the number of patches which motivated the development of hierarchical algorithms based on clustering techniques (see [SS96, PDP96]). Illustrated on say a garden scene, the basic idea is that instead of computing form-factors for all the pairs of leaves, one should not lose too much information by computing form factors for *clusters* of leaves especially in the case of plants located pretty far from one another. But as a result, these clusters —possibly nested— influence the form factors computations between other clusters surface areas as depicted 1(a). And since computing the exact measure of lines leaving a surface area S_1 and reaching a surface area S_2 in the occluded case does not have an exact solution, it would be interesting to have clusters attenuation factors for standard configurations. Such a characterization would also be useful for hierarchical representations of lights as investigated in [PDP96].

A somewhat different problem arises in ray-tracing where the core of any method is the reduction of the number of ray-polygons intersections tests. As observed in [JdL92, Hai96, CP97, CPD95] the best solutions known so far are based on recursive grids and hierarchies of uniform grids. The key point is that by figuring out densely populated areas of the scene (such as the bowl or teapot neighborhood on figure 1(b)), these data structures succeed in partitioning the scene into voxels with low stabbing numbers. In particular it has been shown in [CP97] that the latter data structure was particularly suitable to scenes with natural clusters that is sets of polygons of the 'same' size and 'neighbors', but less appropriated for scenes with more uniform distributions. Examples of such scenes are the kitchen and city depicted on figures 1(b)(c). But here again, it would useful to have a statistical criteria to recognize this kind of scene.

This paper goes in this direction and explores statistics describing the complexity of common scenes used in computer graphics, geographical information systems, etc, and the natural tool to do so is Integral Geometry. Our strategy consists in probing the scene with random entities paying special attention to those statistics that depend on the spatial repartition of the scene objects. By random entities we refer to random lines and planes in $3D$. The reason for this choice is that a random line cutting a scene and split into chords captures some global information on the relative position of the hit objects. The same holds for planes and one could even expect planes to convey a more precise information since e.g. a line can go through a cylinder while a plane cannot ! But as we shall see, for most of the statistics encompassed only the mean is accessible in closed form. That's the reason why this paper devotes a special attention to experiments in an attempt to get a glance of the underlying distribution.

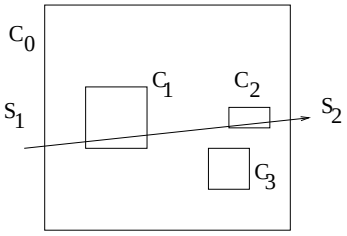

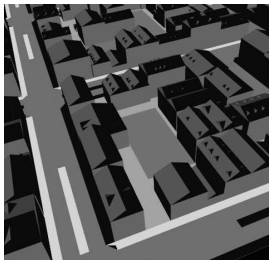

Figure 1: (a)Visibility problem (b)Kitchen model (c)City model

This paper is organized as follows. In the rest of this section we discuss the classical assumption of measures invariant under translations and rotations in the context of non uniform models. In sections 2 and 3 we investigate several results on the intersection of a scene by random lines and planes. And in section 6 we present experimental facts about the statistics considered in the two previous sections.

1.2 Integral geometry, uniform distributions and invariant measures

A major concern when dealing with geometric probability consists in precisely defining what is meant by *at random*. We illustrate this by the Bertrand paradox which addresses the following question: what is

the probability for the length of a random chord of the circle of unit radius to exceed the length of the side of the inscribed equilateral triangle which is $\sqrt{3}$ ([Gneon, KM63]) ?

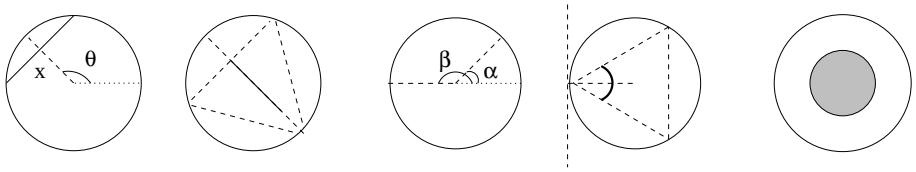

Figure 2: Bertrand's paradox

A first way to get a random chord consists in choosing uniformly at random a direction on the circle and then uniformly at random a point on the corresponding radius: the chord is the line segment whose endpoints are located on the circle and perpendicular to the radius (figure 2(a)). Only the chords that intersect this radius from half of its length to the center of the circle satisfy the condition sought, so that the probability is $1/2$. A second way to get a random chord consists in picking at random two points on the circle (figure 2(b)). Placing a vertex of the equilateral triangle at the first point picked, we can conclude that the probability sought is $1/3$ since the second point has to fall within the cone of measure $\pi/3$ delimited by the triangle vertex. And a third way just consist of fixing the chord midpoint. In this case, this point has to fall within the circle or radius $1/2$ so that we get a probability of $1/4$. We end up with three different values for the same quantity ... which is confusing !

To figure out where the problem is, let a chord be characterized the angle θ it makes with a fixed direction and by the distance x to the center of the circle. The densities associated to the three random schemes are as follows. In the first case, the direction and the point are chosen uniformly at random and independently, so that

$$f_1(x,\theta) = \frac{dx\,d\theta}{2\pi}$$

In the second one, if α and β are the angular coordinates of the chord endpoints, we have $f_2(\alpha,\beta) = d\alpha\,d\beta/(2\pi)^2$. But $\alpha = \theta + \arccos x$ and $\beta = \theta - \arccos x$ with $\theta \in [0, 2\pi)$ and $x \in [-1, 1]$. From this change of variables and by reducing the variation of x to $[0, 1]$ we get

$$f_2(x,\theta) = \frac{dx\,d\theta}{\pi^2\sqrt{1-x^2}}$$

And in the third one, since the circle area is π and the probability for a point to fall in a region of area A is A/π, we have

$$f_3(x,\theta) = \frac{x\,dx\,d\theta}{\pi}$$

It is easily checked that integrating these densities when $\theta \in [0, 2\pi)$ and $x \in [0, 1]$ gives one. As a conclusion, the three results are correct but correspond to different densities of chords, and this paradox shows that the densities of objects considered must be defined carefully. For the applications we are interested in, that is characterizing the complexity of scenes, we will follow the general guideline which consists in using measures invariant by translations and rotations. (f_1 in the example above.) More precisely we will compute an interaction between two kinds of objects: a fixed set of items arbitrarily distributed in $3D$-space (the kitchen polygons in example of figure 1) and a set of random points, lines, planes or whatever ! From now on, by *distribution* we will refer to the distribution of the former data set since the latter must be invariant under the group of rigid motions.

1.3 Notations and elementary results

1.3.1 Particle sets

We suppose the scene is specified as an enumerable set $K = \bigcup_{i=1..n} K_i$ of compact (closed and bounded) subset of the Euclidean space E^3, and by $A(K_i)$ and $V(K_i)$ we denote the surface area and volume of the i^{th} object —that we may also call body or particle. We will use an alternative description of the scene as a set of particles similar to a reference particle within a ratio λ. The volume and surface area of such a λ-object are denoted V_λ and A_λ. The reason for this choice is an interest in more precise statistics

for a subclass of objects —e.g., those whose length lies between λ and $\lambda + d\lambda$, as well as reconstruction purposes as usual in stereology (see [San76, Capter 16]).

We also assume the interiors of the K_i are pairwise of null intersection to make independent their intersection with random figures such as lines and planes. Lastly, we suppose the whole scene is contained in a convex cavity W with surface area $A(W)$ and volume $V(W)$.

1.3.2 Densities of lines and planes in $3D$

The unit sphere in $3D$ is denoted S^2. Due to the invariance requirement under the group of rigid motions, the densities of lines and planes we are interested in are the following ([San76, RPS51, Sol78]):

random direction ω on S^2 is characterized by the pair $(\phi \in [0, 2\pi), \phi \in [0, \pi])$, and the corresponding density is $d\omega = \sin\theta d\theta d\phi$ (4π steradian over S^2);

random line is parameterized by its direction ω on S^2 and by the coordinates (η, ζ) of the intersection point between that line and the plane perpendicular to the direction ω and passing through the origin. The measure is $dG = d\omega d\eta d\zeta$;

random plane π in $3D$ is characterized by its normal vector which is a direction on S^2 and its distance $p > 0$ to the origin, so that the corresponding measure is $d\pi = dpd\omega$.

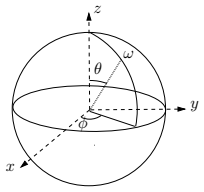

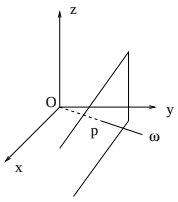

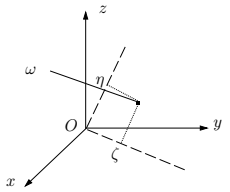

Figure 3: (a)S^2 (b)$3D$ planes (c)$3D$ lines

1.3.3 Projected area of a planar restriction

Let K be a planar bounded set of area F in $3D$. Its projection on a plane whose normal makes the direction ω with the normal of its plane is another bounded set of area $F_\omega = |\cos\omega| F$. By taking the z axis of S^2 to be the normal to the plane containing the object and integrating over S^2 we get $\int_{S^2} F_\omega d\omega = 2\pi F$.

The expected value of the projection area is therefore $F/2$. Applied to all the faces of a convex polyhedra of surface area F, we get an expected value of $F/4$ — known as the Cauchy formula. For more details, see [RPS51, Page 175], [San76, Page 218].

1.3.4 Measure of lines intersecting a body

In $3D$, to compute $\int_{G \cap K \neq \emptyset} dG$, observe that first fixing the direction ω, the coordinates η, ζ can span the area F_ω which is the projection of K on a plane perpendicular to the direction ω. And since we do not consider oriented lines, integrating over half S^2 yields $\mu^G(K) = \int_{S^2/2} f_\omega d\omega$. If K is convex or planar, we have $\mu^G(K) = \pi F/2$ (see [RPS51, Page 201]). Otherwise a fast estimation of the average projected area could be obtained using hardware z-buffer.

1.3.5 Measure of planes intersecting a body, thickness

To compute the measure of planes intersecting a body K, that is $\mu^\pi(K) = \int_{K \cap \pi \neq \emptyset} d\pi$, by first keeping ω fixed, we get $\mu^\pi(K) = \int_{S^2} T(\omega) d\omega$ with $T(\omega) = \int_{\omega\ fixed} dp$. The quantity $T(\omega)$ is called the *thickness* for the direction ω and measures the length of the projection of K along that direction. The integral over all the directions is called the total thickness, or thickness for short. If K is convex, the total thickness is actually equal to the integral of mean curvature, which we recall in the next section. The thickness is also defined for a non connected body. For more details, see [KM63, Page 80], [Sol78, Page 63], [San76, Page 222].

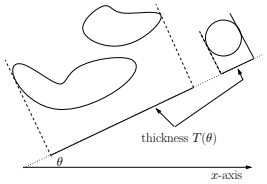

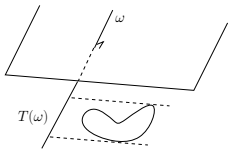

Figure 4: (a)$2D$ thickness (b)$3D$ thickness

1.3.6 Gauss curvature, mean curvature, total curvature

We recall here some important results of differential geometry, and the reader is referred to [McC94, Tho79, HE74, San76] for mode details. Let K be a set whose boundary ∂K is a surface S of class C^2. It is known that at each point p of S there are two principal directions and two **principal curvatures** k_1, k_2. The product of the principal curvatures is the Gauss curvature — Gauss-Kronecker in higher dimension — of the surface defined as follows

$$G = k_1 k_2$$

Geometrically speaking, G is related to the so-called Gauss-Map defined by the surface area spanned on the unit sphere S^2 by the unit normal vectors to the surface S — see fig. 5(a)(b). More precisely, it can be shown that for any elementary surface area ds of S, if $d\omega$ denotes the corresponding surface of S^2 we have

$$G = d\omega/ds$$

For geometric reasons, one may use the values $R_1 = 1/k_1$ and $R_2 = 1/k_2$ called the **principal radii of curvature**, in which case

$$R_1 R_2 = 1/G = ds/d\omega$$

For example, it is easily checked that the Gauss curvatures of a sphere of radius R and of a plane are respectively $1/R^2$ and 0.

From these values, the **mean curvature** M is defined by

$$M = \frac{1}{2}\int_{S^2}(R_1 + R_2)d\omega = \frac{1}{2}\int_S (k_1 + k_2)ds$$

The computation of M values for simple surfaces can be found in [RPS51, pp.178-182], and we have in particular

convex polygon of perimeter L	$M = \pi L/2$
parallelepiped of width a, depth b, height c	$M = \pi(a + b + c)$

Another interesting result we shall use in section 3 is that for a convex surface we have $M = \int_{S^2} T(\omega)d\omega$.

At last, a quantity of interest in section 4 is the **total curvature** Q defined by

$$Q = \int_S k_1 k_2 ds = \int_S \frac{1}{R_1 R_2} ds$$

This quantity is known to be a topological invariant of compact, orientable and without boundary surfaces, related to the Euler characteristic $\chi(S)$ and the genus g of the surface by

$$Q = 2\pi\chi(S) = 4\pi(1 - g)$$

Recalling that for any triangulation $\mathcal{T}$ of the surface S we have $\chi_{\mathcal{T}}(S) = V - E + F$ with V, E, F the numbers of vertices, edges and faces, it is easily seen that $Q = 4\pi$ for a sphere — from fig. 5(c) we get $\chi = 6 - 12 + 8$, $Q = 0$ for a torus, etc.

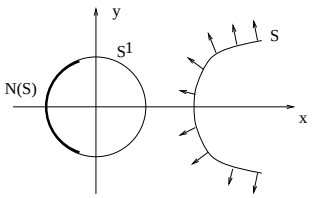

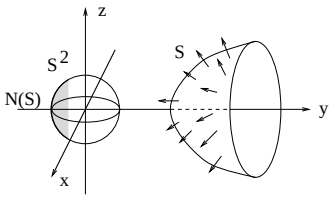

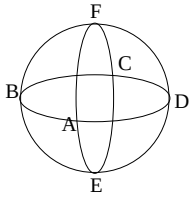

Figure 5: (a)$2D$ Gauss Maps (b)$3D$ Gauss Map (c)Euler characteristic

2 Intersections by lines

In this section, we study the intersection of our scene with random lines. The intersection between a K_i and a line is called a chord, and the complement of all the chords for a given line is called the free path.

2.1 Intersections and chords

Let $\mu^G(K)$ be the measure of the lines intersecting K (that is, any of the K_i). Also let n_{int}^G be the average number of intersections with K of a line *which intersects* W, and $n_{int}^{G\star}$ the average number of intersections with K of a line *which intersects* K (for example, with a single convex body its value would be 2). Then we have

Proposition 1 *The average number of intersection points with K of a line intersecting W and intersecting K are respectively*

$$n_{int}^G = 2\sum A(K_i)/A(W) \text{ and } n_{int}^{G\star} = \pi\sum A(K_i)/\mu^G(K) \tag{1}$$

Proposition 2 *The average length of the sum of the chords per global line and the average length per chord are given by*

$$4\sum_i V(K_i)/A(W) \text{ and } 4\sum_i V(K_i)/\sum_i A(K_i)$$

Proposition 3 *The average mean free path is given by*

$$4\big(V(W) - \sum_i V(K_i)\big) \;/\; \big(A(W) + \sum_i A(K_i)\big)$$

Proof: For prop. 1, each object i is intersected in $\pi A(K_i)$ intersections — see [RPS51, p.201 and p.206], and since the objects are non overlapping the intersections are independent. To complete the proof, it suffices to observe that the measure of lines intersecting W is $\pi A(W)/2$ since W is supposed convex.

For prop. 2 the sum of chords is given by

$$\int_{K\cap G} \sigma d\omega\, d\eta d\zeta = \int_{S^2/2} d\omega \int_{K_\omega} \sigma d\eta d\zeta = 2\pi\sum_i V(K_i)$$

because for each K_i the sum of parallel chords is its volume — [RPS51, p.210], and the measure of lines intersecting W is $\pi A(W)/2$. Hence the first result. As for the second one, we observe that the number of chords is given by half the number of intersections, that is $\pi\sum_i A(K_i)/2$.

As for prop. 3, we want to know the mean free path of a ray, that is, the average length outside a body. But for a ray, the total free length is the length of the ray minus the sum of chords, and since the average of a difference is the difference of averages, we get

$$\frac{4(V(W) - \sum_i V(K_i))}{A(W)}$$

The average length outside a body that is therefore 4 times the unoccupied volume divided by the area of the cavity. To complete the proof it suffices to divide the previous quantity by the average number of chords plus one — to n chords correspond $n+1$ segments outside. □

The result on the number of intersections points was already in [Sbe93], and it should be noticed that for planar objects, the number of objects hit is half of the number of intersection points exactly for convex objects. As we shall see in section 6.1 the theoretical values are matching pretty well the experimentally observed ones. As for the one on the mean free path, it generalizes the one from [San76, Page 42] where the particles are supposed to be uniformly distributed at random. But the common characteristic of these results is to be independent from the objects positions.

2.2 Lines in free space and upper bounds

As soon as the whole scene does not contain surfaces covering the cavity W —in which case a line intersecting W also intersects K, an indicator on the relative position of the particles is the probability for a random line to go through the set K. As observed more than a century ago by Sylvester in [Syl90], getting the exact solution for that problem in dimension two for three bodies is already involved. And as mentioned in 1.1, no exact solution is known in dimension three. In addition to the characterization of section 1.3.4, it can also be shown that the following holds

Proposition 4 *The probability of zero intersections with a random line is given by* $p(0) = 1 - n^G_{int}/n^{G\star}_{int}$

Proof: From proposition 1 we have $\mu^G(K) = \pi A(K)/n^{G\star}_{int}$. But the probability for a line that intersects W to intersect K is given by $\mu^G(K)/\mu^G(W)$. The probability $p(0)$ for a line *not to intersect* K is therefore

$$p(0) = 1 - \frac{\mu^G(K)}{\mu^G(W)} = 1 - \frac{\frac{\pi A(K)}{n^{G\star}_{int}}}{\frac{\pi}{2}A(W)} = 1 - \frac{n^G_{int}}{n^{G\star}_{int}} \tag{2}$$

□

An estimation of this value can be obtained using a z-buffer. Also, getting the distribution of the number of intersections seems to be hopeless ! But a tight upper bound for the probability of i intersections is the following:

Proposition 5 *The probability* $p(i)$ *for a line to intersect* i *bodies in the scene is upper bounded by* $A(K)/(iA(W))$

Proof: By definition of the average number of intersections we have

$$2A(K) \ / \ A(W) = n^G_{int} = 2 \cdot p(2) + 4 \cdot p(4) + \cdots + 2n \cdot p(2n)$$

But since each term of the sum is greater or equal to zero, it is clear that $p(2i) \leq \frac{1}{2i}\frac{2A(K)}{A(W)}, \quad i = 1 \ldots n$ □

These bounds are tight as can be shown by suitably arranging n degenerated objects. Consider for example stacks of pairs or rectangles put side by side, each rectangle being considered as a degenerated body of area A. The probability to have two objects intersected is $A(K)/(2A(W))$ and all the other probabilities are zero.

2.3 The continuous case

We now switch to the second way of describing a scene, that is as a set of particles similar to a reference particle within a ratio λ. We start by the definition of a point density describing the objects present anywhere in the scene:

Definition 1 *We define the density* $H(\lambda, x)$ *as the number of objects of size* λ *at point* x *of the scene. The number of* λ*-objects contained in a volume* V *is given by* $\int_V H(\lambda, x)dV(x)$*, and* N_λ *refers to the number of* λ*-objects in the whole scene i.e.* $\int_{V(W)} H(\lambda, x)dV(x)$

Since any λ-particle adds one to the count of the number of particles, we have $\int_{V_\lambda} H(\lambda, x)dV(x) = 1$ independently of the location of that particle. A natural choice for H is therefore to set $H(\lambda, x) = 1/V_\lambda$ within any object of size λ and zero outside. In other words, $V_\lambda H(\lambda, x) = \chi_\lambda$ i.e. the characteristic function for the union of all objects of size λ. We proceed in the same way for the chords:

Definition 2 *We define the density* $h(\sigma, \lambda, x, G)$ *as the number of objects of size* λ *intersected by a ray* G *with a chord of length* σ*.*

The value of $h(\sigma, \lambda, x, G)$ must equal $1/\sigma$ for a point on a chord of length σ on ray G on a body of size λ and zero otherwise. Indeed, when summing along the chord we have $\int_{G \cap V_\lambda} h(\sigma, \lambda, x, G) dl(G, x) = 1$ whence the value of h. The two densities just defined generalize the densities $H(\lambda)$, $h(\sigma)$, defined in [San76], pp.289-290, which correspond to the number of λ-particles per unit volume, and chords with length σ per unit length, respectively. Also, it is easily checked that

Proposition 6 *For any λ and any G we must have $\int_0^\infty h(\sigma, \lambda, x, G) \sigma d\sigma = V_\lambda H(\lambda, x)$*

These densities can be used to prove results equivalent to the propositions 1, 2 and 3. These results state that the average number of intersections between global lines and the scene is given by $\int A_\lambda N_\lambda d\lambda / A_w$; that the average length of the sum of the chords per ray and the average length of a chord per ray are given by $4 \int V_\lambda N_\lambda d\lambda / A_w$ and $\int V_\lambda N_\lambda d\lambda / \int A_\lambda N_\lambda d\lambda$; and that the average mean free path is given by $4(V_w - \int V_\lambda N_\lambda d\lambda)/(A_w + \int A_\lambda N_\lambda d\lambda)$.
But they can be refined to depend on the two parameters λ and σ as follows:

Proposition 7 *The average number of σ chords for λ-objects over all rays G is given by*

$$m(\sigma, \lambda) = \frac{2}{\pi A(W)} \int \int h(\sigma, \lambda, x, G) dl(G, x) dG$$

The function $\phi(\sigma, \lambda)$ defined as the proportion of σ chords respective to the total of chords is

$$\phi(\sigma, \lambda) = \frac{m(\sigma, \lambda)}{\int m(\sigma, \lambda)} = \frac{2}{\pi A_\lambda N_\lambda} \int \int h(\sigma, \lambda, x, G) dl(G, x) dG$$

Another interesting property of these densities is that one can get information on H from h, that is on the three-dimensional repartition of the set of particles from its section with random lines. To see how, let $\phi(\sigma) = \phi(\sigma, 1)$ be the proportion of chords on K_1 which lie between σ and $\sigma + \mathrm{d}\sigma$, and let σ_m denote the greatest chord cut on K_1. The following proposition generalizes the one in [San76], pp.289-290:

Proposition 8

$$\int_{\lambda = \sigma/\sigma_m}^\infty \int \lambda \phi(\sigma/\lambda) H(\lambda, x) dV(x) d\lambda = 1/(\pi A_1) \int \int \int h(\sigma, \lambda, x, G) dl(G, x) dG d\lambda$$

Proof: For K_λ we have $\phi(\sigma, \lambda) d\sigma = \phi(\sigma/\lambda, 1) d(\sigma\lambda) = \lambda^{-1} \phi(\sigma/\lambda) d\sigma$. On the other hand, $A_\lambda = \lambda^2 A_1$. Observing that $N_\lambda = \int_{V(W)} H(\lambda, x) dV(x)$ completes the proof. □

3 Intersections by planes

3.1 Intersections and sections

Consider the set K as in the previous section and let $\mu^\pi(K)$ be the measure of the planes which intersect any of the K_i. Also let n_{int}^π be the average number of objects of K intersected with a plane which intersects the cavity W, and $n_{int}^{\pi\star}$ the average number of intersections with K of a plane which intersects K. We have:

Proposition 9 *The average number of objects in K intersected by a plane intersecting W and intersecting K are respectively*

$$n_{int}^\pi = \sum_i T(K_i)/M(W) \text{ and } n_{int}^{\pi\star} = \sum_i T(K_i)/T(K) \tag{3}$$

Proposition 10 *The average section and perimeter with K for a random plane intersecting W are given by*

$$2\pi \sum_i V(K_i)/M(W) \text{ and } \pi^2 \sum_i A(K_i)/2M(W) \tag{4}$$

Proposition 11 *The average section and perimeter with an object of K for a random plane intersecting W are given by*

$$\frac{2\pi \sum_i V(K_i)}{\sum_i T(K_i)} \text{ and } \frac{\pi^2 \sum_i A(K_i)}{2 \sum_i T(K_i)} \tag{5}$$

Proof: For prop. 9, as recalled in section 1.3.5, each object i is intersected by $T(K_i)$ planes, hence the result.

For prop. 10, given any direction ω and any object K_i, the sum of the sections of all planes parallel to that direction with K_i gives $V(K_i)$. But we have 2π directions, hence the result. For the second result, it is enough to follow the proof in [RPS51], pp.221-223, considering that $\sum_i A(K_i)$ is the area of K.

As for prop. 11, it results from the division of the expression (4) by the value of n^{π}_{int} given by expression (3). □

In particular, if all objects in K are convex one can replace $T(K_i)$ by $M(K_i)$. Exactly as with the lines, the important fact with these statistics is to be independent of the objects distribution.

3.2 Planes in free space and upper bounds

The results are similar to the lines case. Indeed, since the world cavity W is supposed to be convex we have $\mu^{\pi}(W) = M(W)$. Then, using the thickness $T(K)$ of the set K we get

Proposition 12 *The probability for a plane that, intersecting W, does not intersects K, is given by*

$$p(0) = 1 - T(K)/M(W) = 1 - n^{\pi}_{int}/n^{\pi\star}_{int} \tag{6}$$

Proof: The probability of intersection is simply the quotient of the measures of the planes intersecting K and W, that is $T(K)/M(W)$ hence the result. □

The importance of this result is that we can have an estimation of $p(0)$ with a repeated application of a scan-line algorithm, which can be hardware implemented.
We now give without proof the following proposition analogous to the one in the previous section:

Proposition 13 *The probability for a random plane to intersect i objects of K is bounded by $T(K)/(iM(W))$*

3.3 The continuous case

To refine the previous results as in the lines case, we first define a discrete density characterizing the sections of area s — also called s sections — between a plane and an object:

Definition 3 *We define the density $h^{\pi}(s, \lambda, x, \pi)$ as the number of objects of size λ intersected by a plane π with a section of area s.*

The value of $h^{\pi}(s, \lambda, x, \pi)$ must equal $1/s$ for a point on a section of area s on plane π on a body of size λ and zero otherwise. Indeed, when summing along the section we have $\int_{\pi \cap V_\lambda} h^{\pi}(s, \lambda, x, \pi) dA(\pi, x) = 1$ whence the value of h. The density just defined generalizes the density $h^{\pi}(s)$, defined in [San76], pp.286-287, which corresponds to the number of sections with area s per unit area. Exactly as with the lines case one can get the results of the discrete case. We skip this discussion and present specific results to λ-objects and s-sections:

Proposition 14 *For a given λ, the average number of s sections over all planes π is given by*

$$m^{\pi}(s, \lambda) = \frac{1}{M_w} \int \int h^{\pi}(s, \lambda, x, \pi) dA(\pi, x) d\pi$$

The function $\phi^{\pi}(s, \lambda)$ defined as the proportion of s sections respective to the total of sections is

$$\phi^{\pi}(s, \lambda) = \frac{m^{\pi}(s, \lambda)}{\int m^{\pi}(s, \lambda) ds} = \frac{1}{T_\lambda N_\lambda} \int \int h^{\pi}(s, \lambda, x, \pi) dA(\pi, x) d\pi$$

Here again, the stereology purposes of [San76, pp.286-287] can also be generalized. To see how, let $\phi^\pi(s) = \phi^\pi(s,1)$ be the proportion of sections on K_1 which lie between s and $s + \mathrm{d}s$, and let s_m refer to the greatest section cut on K_1. The following proposition generalizes the one in [San76], pp.286-287.

Proposition 15

$$\int_{\lambda=\sqrt{s/s_m}}^{\infty} \int \lambda^{-1} \phi^\pi(\frac{s}{\lambda^2}) H(\lambda, x) dV(x) d\lambda = \frac{1}{T_1} \int \int \int h^\pi(s, \lambda, x, \pi) dA(\pi, x) d\pi d\lambda$$

Proof: For K_λ we have $\phi^\pi(s,\lambda)ds = \phi^\pi(s/\lambda^2, 1)d(s/\lambda^2) = \lambda^{-2}\phi^\pi(s/\lambda^2)ds$ On the other hand, $T_\lambda = \lambda T_1$, and observing that $N_\lambda = \int_{V_w} H(\lambda, x)dV(x)$ completes the proof. □

3.4 Intermezzo: a thickness-related statistic

As observed in section 1.3.5, the thickness along a line of the set K is equal to the length of the objects' projections along that line. Of course, the projection of two or several objects may overlap one-another, and a question of interest is to know whether or not measuring this overlapping can give information on the objects' overall distribution. More precisely:

Definition 4 *Let a one-dimensional arrangement of n line segments be a set of n line segments with distinct extremities on some line L. We define the* overlap number *of this arrangement as the sum over all the endpoints, of the number of line segments interiors these endpoints are contained in*

An example of arrangement of 3 line segments $\{(a_1, a_2), (b_1, b_2), (c_1, c_2)\}$ is depicted on fig. 6, and the corresponding overlap number is $0 + 1 + 2 + 2 + 1 + 0 = 6$. From [Caz97], the following proposition is straightforward:

Proposition 16 *The average overlap number τ_n of a random arrangement of n line segments is given by*

$$\tau_n = \frac{4n^3/3 - 2n^2 + 2n/3}{2n - 1}$$

So that a natural way to use this overlapping measure consists in comparing the theoretical value τ_n with an experimental value $\varepsilon\tau_n$ computed by averaging the overlap numbers of random arrangements obtained by projecting the scene objects onto random lines. As we shall see in section 6.3, if the fingerprint role of this statistic is not obvious, a surprising property lies in its stability under uniform sampling.

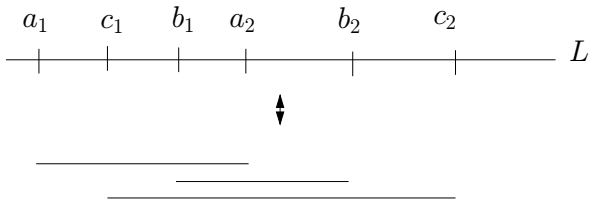

Figure 6: Arrangement of line segments

4 Intersections with a lattice of cubes

So far, we considered a fixed scene and probed it with random lines and planes. A dual formulation of the problem consists in moving the scene over a fixed geometric figure and computing statistics for the configurations thus obtained. This is particularly interesting since choosing the figure as a grid-like lattice of side a and counting the number of intersections could intuitively give information about densely populated areas called clusters in [CP97]. The difficulty we have to face here are double: first how do we specify the way the K_i are moved around ? second, how do we deal with the non uniform distribution of the K_i ? It actually turns out that much of the previous work ([San76, Chapters 6,12,15]) specifies the motion of the objects by the so-called kinematic density relying on distance preserving affine transformations. And the measures associated to that subgroup of the affine group are always invariant differential forms. In other words, in order to characterize non uniform distributions of particles by

assigning a non uniform position and orientation to a reference particle, one has to reinvent the wheel! We therefore present a result based on a transformation of the scene into a single object moved around by the usual kinematic density:

Proposition 17 *If all the K_i are topological balls, the expected number of intersection cells between a cubic lattice of side a and the scene K is upper bounded by*

$$E(N) \leq 1 + \frac{\sum_i V(K_i)}{a^3} + \frac{1}{4\pi}\left(\frac{3\pi\sum_i A(K_i)}{a^2} + \frac{6(\sum_i M(K_i) + \pi b)}{a}\right) \tag{7}$$

where b is the cumulated length of $n-1$ line segments connecting the K_i into a tree

Proof: For a topological ball B ([San76, p.274]), this number is bounded by

$$E(N) \leq \frac{1}{4\pi}\left(Q(B) + \frac{4\pi V(B)}{a^3} + \frac{3\pi A(B)}{a^2} + \frac{6M(B)}{a}\right) \tag{8}$$

with $Q(B)$ the total curvature mentioned in 1.3.6. The trick therefore consists in changing K into a new body $K^\star$ which is a topological ball. To do so, we just have to find a spanning tree over the K_i and add $n-1$ rods of arbitrarily small diameter between the K_i thus connected —note that adding n or more rods would result in a cycle so that we would not have a topological ball anymore. Let b the total length of these rods. Plugging the following values into eq. (8) completes the proof

$$Q(K^\star) = 4\pi, V(K^\star) = \sum_i V(K_i), \quad A(K^\star) = \sum_i A(K_i), M(K^\star) = \sum_i M(K_i) + \pi b$$

□

If the particles are located far away from one another, the previous expression will result in a too high value. But observe that this can be detected by removing all the rods of length greater than $a\sqrt{3}$. The previous formula is still valid but the first term has to be replaced by the the number of connected components produced.

5 Test scenes

We refer the reader to [CP97].

6 Experiments

For most of the statistics considered so far, we saw that the only closed form integral geometers had been able to come up with was the expectation, which in many cases does not depend upon the objects' relative positions. This already gives very interesting information, but two open questions of major interest are related to the distributions associated to these expectations, and also to higher order moments.

As a first step in this direction and for selected statistics studied in sections 2 and 3, we present thereafter two kinds of experimental results. Firstly, we compare the expected theoretical values with experimentally observed ones, together with experimental standard deviations. Secondly, we plot the random variables densities and cumulated distribution functions. For a given scene and a given variable, these two functions are depicted on the same chart but are easily distinguished since the latter is increasing and ends up with the value 1.

6.1 Random lines statistics

6.1.1 Random lines generation and statistics studied

The statistics we consider are the number of intersections, the probability p_0 measuring the chances for a line to miss all the objects, and a free path related statistic — see section 2. Before discussing them, we first observe — as shown for example in [Sbe93, Sol78] — that generating a random line uniformly in S^2 just requires two random points on the surface of the sphere. This result is kind of surprising since the uniformity does not hold in dimension two according to the Bertrand's paradox. Generating uniformly

distributed random lines crossing a scene can therefore be done by generating such lines in the sphere containing the scene bounding box and discarding those that do not hit this box.

For the number of intersection points statistic, the value n_{int}^G is given by prop. 1. Computing this number for a polygonal scene is straightforward since the area of a polygon P with vertices $(v_0, \ldots, v_{n-1})$ is given by

$$\mathcal{A}(P) = \mathcal{A}(p, v_0, v_1) + \mathcal{A}(p, v_1, v_2) + \ldots + \mathcal{A}(p, v_{n-1}, v_0) \tag{9}$$

with p any point lying in the polygon plane and $\mathcal{A}(p, v_0, v_1)$ the area of the triangle (p, v_0, v_1) —see [O'R94, p. 24]. As for the computation of the experimental expectation and standard deviation en_{int}^G and σen_{int}^G, it is sufficient to test all the polygons for intersection with the query rays.

For the p_0 statistic, we saw that the theoretical value derived in proposition 2 was not amenable to an easy computation. On the other side, getting an experimental value for it just requires dividing the number of rays missing all the scene objects by the total number of rays casted.

As for the free path related statistic, since for polygonal scenes the whole ray except the intersection points lies in free space, we consider the length of the line segments delimited by the intersection points with the objects and the scene bounding box. An example of ray split into four line segments of lengths l_1, l_2, l_3, l_4 is depicted on figure 7(b). Over a set of rays casted, each of these lengths is affected the same weight i.e. 1, and to normalize the results all the lengths were divided by the largest length observed. The experimentally observed expectation and standard deviation of this random variable CL are denoted μCL and σCL in the sequel.

6.1.2 Results

All the tests were performed by casting 50,000 random lines on the scenes. Figure 7(a) shows 200 such lines for the Berkeley Computer science building. Reporting all the hits for a given ray was done using a uniform grid — see [CPD95]. A recursive one would have been more efficient but the goal here is to characterize scenes properties as a pre-processing. The results are presented on table 1 and figures 8, 9, 10 and 12:

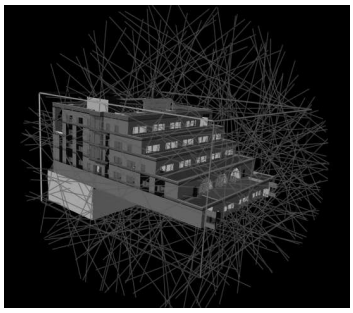

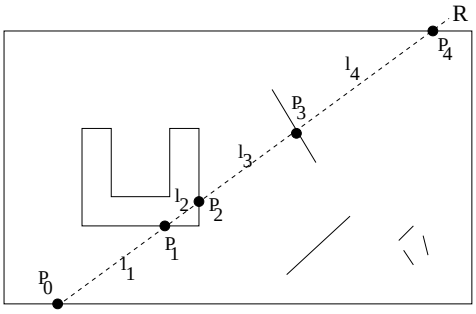

Figure 7: Random lines and chords statistics

Scene	#polys	p_0	n_{int}^G	en_{int}^G	σen_{int}^G	μCL	σCL
Kitchen	20947	0.4	3.66	3.7	4.7	0.2	0.1
CSB walls	32811	0.35	6.66	6.03	7.17	0.26	0.17
CSB 3^{rd} floor	117605	0.15	3.5	3.2	3.6	0.09	0.1
City	52136	0.15	2.0	2.02	2.24	0.02	0.05
Garden	45293	0.83	0.31	0.3	0.96	0.3	0.19

Table 1: Statistics on random lines and chords

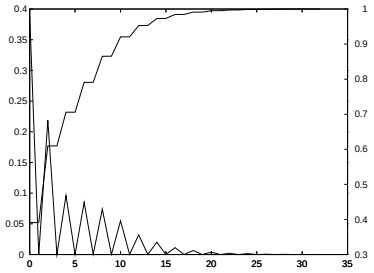
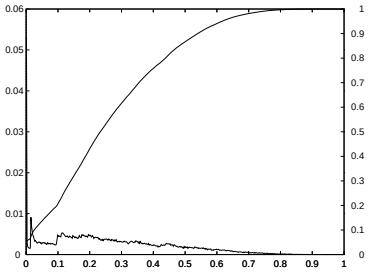

Figure 8: Kitchen stats (a)Number of intersections (b)CL distribution

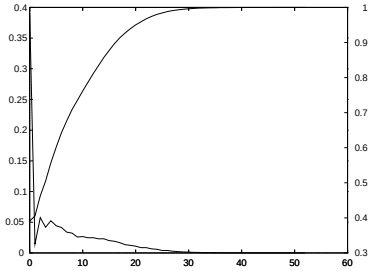
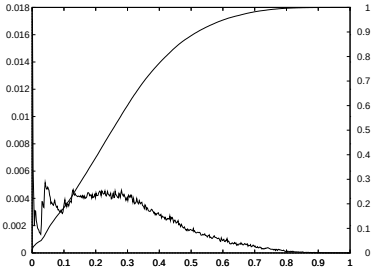

Figure 9: CSB walls stats (a)Number of intersections (b)CL distribution

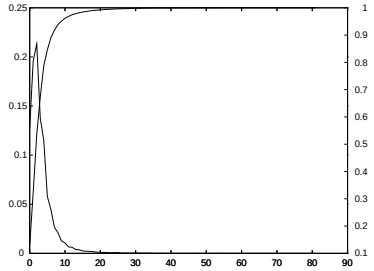
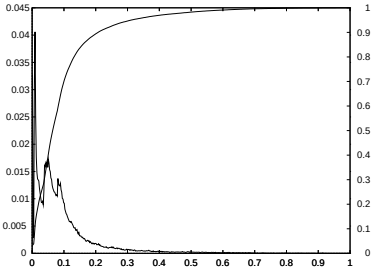

Figure 10: CSB third floor stats (a)Number of intersections (b)CL distribution

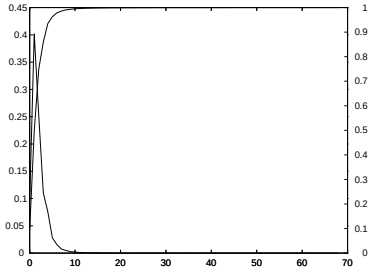
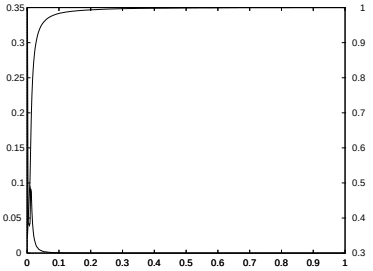

Figure 11: City stats (a)Number of intersections (b)CL distribution

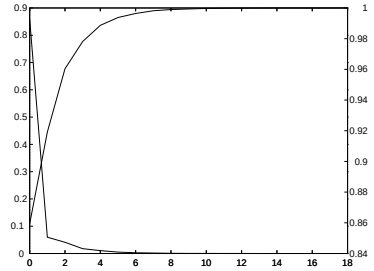
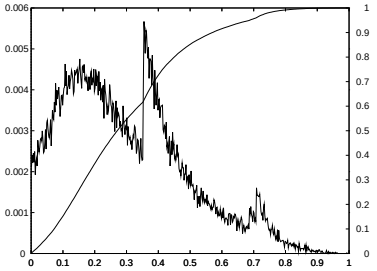

Figure 12: Garden stats (a)Number of intersections (b)CL distribution

For the only statistic where the theoretical and experimental values are available, that is the number of intersections, a very satisfying observation is that the theory matches the practice pretty well. Indeed, as shown on table 1, n_{int}^G and en_{int}^G are within a few percents. The discrepancy is a bit bigger for the CSB scenes, and there are at least two candidates explanations. It could be that some polygons of the models are not simple polygons in which case the surface area computation of eq. (9) does not hold. Or it could be that the rate on convergence of the en_{int}^G estimator is more sensitive to these scenes. More interesting are the other quantities, and we analyze them now in order of increasing difficulty.

For the **city**, things are pretty easy. Most of the lines hitting the scene bounding box also hit the scene and the chords lengths are uniformly small which means that the scene objects are uniformly placed and close from one another —otherwise more lines would miss the set K. Also the average number of intersections with reference to the number of polygons in the scenes probably accounts for a $2,5D$ distribution.

For the **garden** the situation is not more involved. Most of the lines are missing the set K which means that the scene is made of small objects, and the high variability of the chord lengths means that these objects are scattered all over the place.

But for the **CSB 3^{rd} floor, the CSB walls and the Kitchen**, things get a little trickier. By first observing the chords length diagrams we see that there are more shorter chords for the CSB 3^{rd} floor than for the two other scenes which means that the scene space probably exhibits a thinner subdivision. On the other hand and with reference to the total number of polygons, the third floor has a low average number of intersections. An explanation is that most of the objects are clustered in some dense areas and are not hit very often. As for the CSB walls and the kitchen, they exhibit a similar behavior in terms of average and standard deviation, excepted that the kitchen diagrams show some striking zigzags ! In particular any ray has an even number of hits. This is due to the fact that all the scene polygons are arranged to form closed surfaces. Instead of reporting the number of polygonal hits, we could have reported the number of objects hits, but this would fail in giving any information on the spatial repartition of all these polygons —a great number of tiny polygons arranged to form a non convex surface that would result in a great number of hits would count for one! From the zizgag observation we can therefore deduce that the *independent* number of polygons hit in the kitchen is smaller in a significant factor to the one of the CSB walls scene.

6.2 Random planes statistics

6.2.1 Random planes generation and statistics studied

From the density of planes recalled in section 1.3.2, generating a random plane is straightforward: we need a direction i.e. a point on S^2, and a positive distance for the distance from the plane to the coordinate system origin. Now, to have these planes uniformly distributed at random in the volume containing the scene, it suffices to generate planes in the sphere containing the scene bounding box and centered at the center point of this box, and to discard those that do not cross the box. An arrangement of 10 such planes for the kitchen scene is shown on fig. 13(a) — note that the planes have been clipped against the scene bounding box.

Due to the difficulty of maintaining a polygonal map describing the scene objects projection on a plane, we just report results related to the number of intersections between a random plane and the scene. The theoretical expectation n_{int}^{π} has been computed in prop. 9. For the total thickness of object K_i we used the corresponding mean curvature given in 1.3.6, as if K_i was convex. As we shall see with the experiments, for our test scenes where more than 95% of polygons are triangles and squares, these two approximations do not result in significant errors. Before discussing the results, we should point out that by en_{int}^{π} and σen_{int}^{π} we refer to the experimentally observed expectation and standard deviation of the number of intersections of the scene with a random plane.

6.2.2 Results

All the tests were performed with 50,000 random planes. The results are displayed on table 2 and figures 13(b), 14 and 15.

Scene	p_0	n^{π}_{int}	en^{π}_{int}	σen^{π}_{int}
Kitchen	0.17	152.909	153.528	188.117
CSB 3^{rd} floor	0.04	332.738	332.039	332.556
CSB walls	0.18	524.739	522.565	531.268
City	0.03	291.584	291.802	172.092
Garden	0.26	145.542	147.003	161.073

Table 2: Statistics on 50000 random planes

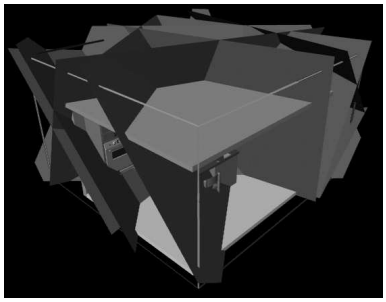

Figure 13: (a)Random planes crossing the kitchen

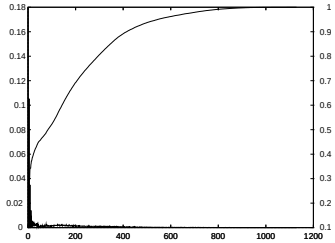

(b)Kitchen stats

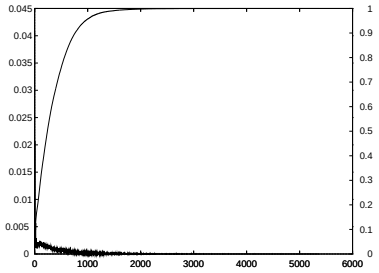

Figure 14: (a)3^{rd} floor

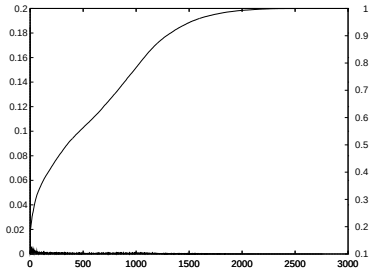

(b)CSB walls

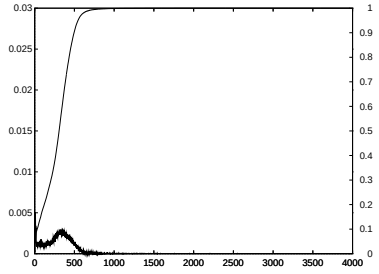

Figure 15: (a)City

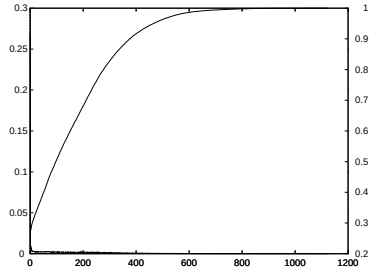

(b)Garden

Exactly as for the lines case, a positive point is that the values of n^{π}_{int} and en^{π}_{int} are very close to one another. Concerning the p_0 statistic, the lower values are obtained for the city and CSB 3^{rd} floor scenes, which is not surprising since these two scenes are contained in an axis aligned parallelepiped so that any plane crossing that box also intersect some object with high probability. Intermediate values are obtained for the kitchen and the CSB walls. Since for these two scenes the surface of the scene convex hull mainly consists of scene polygons — in particular those corresponding to the walls, this just means that there is a noticeable discrepancy between the scene convex hull volume and the scene bounding box volume. The highest value is obtained for the garden scene which is not very surprising.

Concerning the standard deviation σen^{π}_{int}, it should be noticed that the values of en^{π}_{int} and σen^{π}_{int} are of the same order of magnitude for all the scenes but the city one. For that one, having a much lower standard deviation probably captures some notion of uniformity. This is interesting especially since an equivalent property does not hold for the lines statistics.

As for the distribution of the number of intersections, the interpretation is not that easy!

6.3 The thickness-related statistic

In section 3.4, we defined the average overlap number τ_n, and our concern in this section is to study the ratio $\rho_n = \tau_n/\varepsilon\tau_n$, with $\varepsilon\tau_n$ the experimental value associated to τ_n.

The qualitative information sought is related to the objects' size as well as their relative placement. Indeed, tiny objects scattered all over the place are unlikely to overlap one-another when projected on a line. On the opposite, bigger objects evenly distributed in $3D$ are likely to overlap. Also, if this quantity is a good fingerprint of a given scene, one could expect its value to be stable under uniform sampling. Indeed, when picking objects at random, one gets a 'picture' of the scene at different levels of detail because those highly populated areas of the scene are also those that receive the highest representation in the sample. This is illustrated on figures 16 and 17. In particular, with only 2% of objects one can already guess that bowl, plates, teapot and tops of the chairs.

The ratios ρ_n for 1%, 5%, 20%, 40%, 80% and 100% objects of the scene, as well as 50 and 500 random rays are presented on table 3.

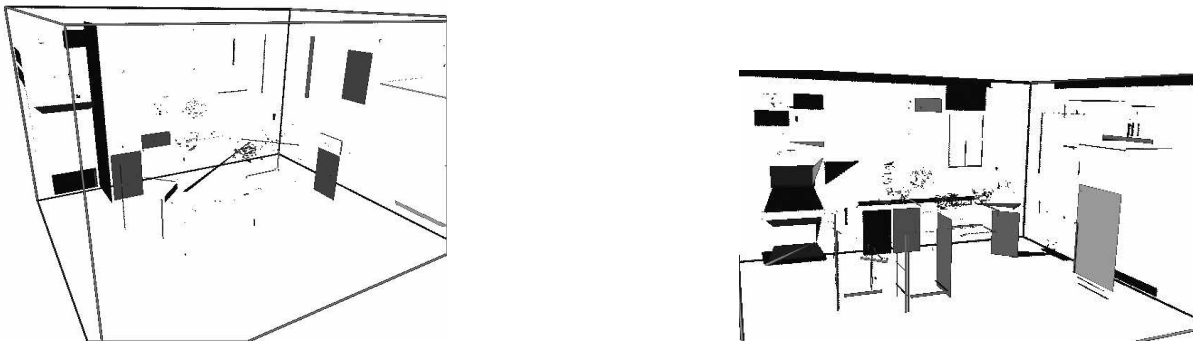

Figure 16: Uniformly sampling the kitchen scene: 2% and 5% of objects

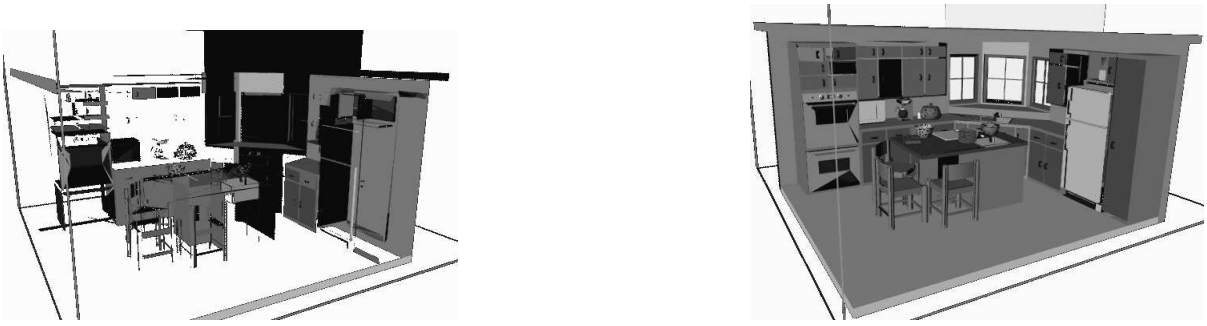

Figure 17: Uniformly sampling the kitchen scene: 20% and 80% of objects

Scene	# rays	%obj	0.01	0.05	0.1	0.2	0.4	0.8	1
Kitchen	50		0.0698	0.0652	0.0673	0.0709	0.0654	0.0688	0.0680
	500		0.0615	0.0645	0.0692	0.0669	0.0685	0.0689	0.0687
CSB 3^{rd} floor	50		0.0288	0.0240	0.0190	0.0212	0.0194	0.0203	0.0225
	500		0.0214	0.0210	0.0217	0.0221	0.0214	0.0215	0.0219
CSB Walls	50		0.0922	0.1010	0.0916	0.0936	0.0996	0.0974	0.0984
	500		0.0978	0.0996	0.1000	0.0948	0.0992	0.0980	0.098
City	50		0.0277	0.0270	0.0260	0.0243	0.0240	0.0242	0.0260
	500		0.0265	0.0251	0.0263	0.0261	0.0255	0.0266	0.0263
Garden	50		0.0226	0.0219	0.0216	0.0212	0.0213	0.0213	0.0209
	500		0.0209	0.0213	0.0227	0.0216	0.0220	0.0216	0.0218

Table 3: The $\rho_n = \tau_n/\varepsilon\tau_n$ statistic

The most striking observation is the stability of ρ_n since we get values within 10% or so for the whole scene and 1% of its objects. On the other hand, ρ_n fails in giving obvious information of the objects' spatial distribution since we have the ordering

$$\rho_{garden} < \rho_{CSB\ 3^{rd}floor} < \rho_{city} < \rho_{kitchen} < \rho_{CSB\ walls}$$

and in terms of clustering ability one would expect

$$\{\rho_{CSB\ 3^{rd}floor}, \rho_{kitchen}, \rho_{garden}\} < \{\rho_{city}, \rho_{CSB\ walls}\}$$

7 Conclusion

In this paper we systematically studied the interaction between general three dimensional distributions of non overlapping particles and random lines, random planes, and cubic lattices. The results obtained generalise Integral Geometry results to non uniform distributions of objects and shed light on which tools are of interest to investigate visibility problems as well as scenes classification purposes in computer graphics. An important contribution of this paper is to show through a careful experimental study, that the theory and practice are in excellent correspondence. This legitimates the scene model we used and should motivate future work.

In particular, the interest devoted to the distributions attached to the expectations gives pretty disappointing results since it seems very difficult to quantify them in terms of scenes classification for example. Major emphasis should therefore be put on devising more informative statistics. In doing so, the stability of these statistics under sampling should also be carefully addressed since this is a major issue when dealing with very big models.

Other questions of major interest and of more theoretical flavor are the following. Firstly, how easily can one perform average case analysis for the lattices with non invariant kinematic densities over the subgroup of distance preserving affine transformations ? Secondly, which kind of results can one come up with by getting rid of the non-overlapping hypothesis between the particles ? By doing so, we could define continuous densities equivalent to the discrete density H defined in this paper and probably get more analytical results. Thirdly, can any rate of convergence be stated for estimators of the statistics studied in this paper? This question is of special interest in connection with the work of V. Vapnik and A. Chervonenkis ([VC71]) which has already received a huge echo in the CG community.

ACKNOWLEDGMENTS: Mateu Sbert was supported by the grants TIC 95-0614-C03-03 and 1995BEAI20012 respectively from the Spanish and the Catalan governments. The authors wish to thank Claude Puech and Xavier Pueyo to have made this collaboration possible.

References

[Caz97] F. Cazals. Combinatorial properties of one-dimensional arrangements. *Experimental Mathematics*, 6(1), 1997.

[Cha89] B. Chazelle. Lower bounds on the complexity of polytope range searching. *J. of the A.M.S*, 2(4), 1989.

[CP97] F. Cazals and C. Puech. Bucket-like space partitioning data structures with applications to ray-tracing. In 13^{th} *ACM Symposium on Computational Geometry*, Nice, 1997.

[CPD95] F. Cazals, C. Puech, and G. Drettakis. Filtering, clustering and hierarchy construction: a new solution for ray tracing complex scenes. *Computer Graphics Forum*, 14(3), 1995.

[Dev86] L. Devroye. *Lecture Notes on Bucket Algorithms.* Birkauser, 1986.

[For96] CG Task Force. Application challenges to computational geometry. Technical Report TR-521-96, Princeton University, 1996.

[Gneon] B. Gnedenko. *The Theory of Probability.* Chelsea, 1989 (Fith Edition).

[Hai96] E. Haines. Personal communication. 1996.

[HE74] E. Harding and D. Kendall (Editors). *Stochastic geometry : a tribute to the memory of Rollo Davidson.* Wiley, 1974.

[JdL92] Erik Jansen and Win de Leeuw. Recursive ray traversal. *Ray Tracing News (available at nic.funet.fi:/pub/graphics/misc/RTNews)*, 5(1), 1992.

[KM63] Kendall and Moran. *Geometric Probability.* Hafner Publishing Company, 1963.

[McC94] J. McCleary. *Geometry from a differentiable viewpoint.* Cambridge Univ. Press, 1994.

[Mor66] P. Moran. A note on recent research in geometrical probability. *J. Appl. Prob.*, 3:453–463, 1966.

[Mor69] P. Moran. A second note on recent research in geometrical probability. *Adv. Appl. Prob.*, 1:73–89, 1969.

[O'R94] J. O'Rourke. *Computational Geometry in C.* Cambridge University Press, 1994.

[PDP96] E. Paquette, G. Drettakis, and P. Poulain. Hierarchical representation of lights for ray-tracing. *In preparation*, 1996.

[RPS51] J. Rey-Pastor and A.L. Santaló. *Geometria integral.* Espasa-Calpe Madrid, 1951.

[San76] A.L. Santaló. *Integral Geometry and Geometric Probability.* Addison-Wesley, 1976.

[Sbe93] M. Sbert. An integral geometry based method for fast form-factor computation. *Computer Graphics Forum - Eurographics'93*, 12(3), 1993.

[SD95] P. Su and S. Drysdale. A comparison of sequential delaunay triangulation algorithms. In *Proc. of the* 11^{th} *ACM Symp. on Computational Geometry*, pages 61–70, 1995.

[Sil95] F. Sillion. A unified hierarchical algorithm for global illumination with scattering volumes and object clusters. *IEEE Transactions on Visualization and Computer Graphics*, 1(3), 1995.

[Sol78] H. Solomon. *Geometric probability.* SIAM - CBMS 28, 1978.

[SS96] C. Soler and F. Sillion. Accurate error bounds for multi-resolution visibility. In 7^{th} *Eurographics Workshop on rendering*, pages 61–70, Porto, 1996.

[SW93] R. Schneider and J. Wieacker. Integral geometry. In P.M. Gruber and J.M. Mills, editors, *Handbook of convex geometry.* Elsevier, 1993.

[Syl90] J.J Sylvester. On a funicular solution of buffon's needle problem. *Acta Math.*, 14:185–205, 1890.

[Tho79] J.A. Thorpe. *Elementary topics in differential geometry.* Springer, 1979.

[VC71] N. Vapnik and A. Chervonenkis. On the uniform convergence of relative frequencies of events to their probabilities. *Theory of probability and its Applications (SIAM)*, 16(2):264–280, 1971.

[WW93] W. Weil and J. Wieacker. Stochastic geometry. In P.M. Gruber and J.M. Mills, editors, *Handbook of convex geometry.* Elsevier, 1993.

Unité de recherche INRIA Lorraine, Technopôle de Nancy-Brabois, Campus scientifique,
615 rue du Jardin Botanique, BP 101, 54600 VILLERS LÈS NANCY
Unité de recherche INRIA Rennes, Irisa, Campus universitaire de Beaulieu, 35042 RENNES Cedex
Unité de recherche INRIA Rhône-Alpes, 655, avenue de l'Europe, 38330 MONTBONNOT ST MARTIN
Unité de recherche INRIA Rocquencourt, Domaine de Voluceau, Rocquencourt, BP 105, 78153 LE CHESNAY Cedex
Unité de recherche INRIA Sophia-Antipolis, 2004 route des Lucioles, BP 93, 06902 SOPHIA-ANTIPOLIS Cedex

Éditeur
INRIA, Domaine de Voluceau, Rocquencourt, BP 105, 78153 LE CHESNAY Cedex (France)
http://www.inria.fr
ISSN 0249-6399